Non-linear free vibrations and post-buckling analysis of shear flexible functionally graded beams

K. Sanjay Anandrao[*1], R.K. Gupta[1a], P. Ramchandran[2a] and G. Venkateswara Rao[3b]

[1]*Advanced Systems Laboratory, Kanchanbagh, Hyderabad-500058, India*
[2]*DRDL, Kanchanbagh, Hyderabad-500058, India*
[3]*Department of Mechanical Engineering, Vardhaman College of Engineering, Shamshabad,
Hyderabad-501218, India*

Abstract. Large amplitude free vibration and thermal post-buckling of shear flexible Functionally Graded Material (FGM) beams is studied using finite element formulation based on first order Timoshenko beam theory. Classical boundary conditions are considered. The ends are assumed to be axially immovable. The von-Karman type strain-displacement relations are used to account for geometric non-linearity. For all the boundary conditions considered, hardening type of non-linearity is observed. For large amplitude vibration of FGM beams, a comprehensive study has been carried out with various lengths to height ratios, maximum lateral amplitude to radius of gyration ratios, volume fraction exponents and boundary conditions. It is observed that, for FGM beams, the non-linear frequencies are dependent on the sign of the vibration amplitudes. For thermal post-buckling of FGM beams, the effect of shear flexibility on the structural response is discussed in detail for different volume fraction exponents, length to height ratios and boundary conditions. The effect of shear flexibility is observed to be predominant for clamped beam as compared to simply supported beam.

Keywords: functionally graded materials; large amplitude vibrations; post-buckling; finite element analysis; shear flexibility; von-Kármán geometric non-linearity; Newton-Raphson method

1. Introduction

The concept of Functionally Graded Materials (FGM) was proposed by Japanese scientists (Koizumi 1993) as a means of preparing thermal barrier materials. In FGM, the micro-structural composition of the constituent materials is continuously varied (Aboudi *et al.* 1999). The choice of the constituent materials and the variation of these materials are decided by the desired application to obtain required distribution of material properties such as Young's modulus, density, coefficient of thermal expansion etc. in the required direction. FGM structures can be efficiently used in a variety of structural applications such as advanced aircraft and aerospace engines, computer circuit boards, re-entry vehicles, nuclear components, steel plants, automobiles and other engineering

*Corresponding author, Scientist, E-mail: sanjayanandkhalane@gmail.com
[a]Scientist
[b]Distinguished Professor

applications where structures are subjected to severe thermal loads. The metal-ceramic FGM components, in particular, are best suited for these applications. Structural members such as beams are basic components in these applications. The design of FGM structures, unlike homogenous structures, is controlled by many parameters. This necessitates understanding and development of proper analysis techniques to fully utilize their potential.

Severe dynamic environment, which may exist in some of the above applications, can lead to large amplitude vibrations of beams. This requires a thorough knowledge of the dynamic behavior of the structure. Further, for a beam under thermal load, a linear buckling analysis gives critical value of temperature for prescribed boundary conditions. However, these structures can withstand considerable additional thermal load before ultimate load is reached. This necessitates having an in-depth understanding of the post-buckling response of these structures so as to effectively utilize their additional load carrying capability provided that the large deformations do not interfere with functional requirement of the structure.

The large amplitude vibration of uniform, homogeneous and isotropic beams is studied extensively (Woinowsky-Krieger 1950, Srinivasan 1965, Rao and Raju 1978, Raju and Rao 1984, Singh 1990, Sathyamoorthy 1998, Rao and Raju 2002, Raju and Rao 2005, Rao 2007). Various formulations and solution techniques were used in these studies. Many of the researchers have studied vibrations of FGM beams. Chakraborty *et al.* (2003) developed a new beam finite element for analysis of functionally graded beams. They considered static, free vibration and wave propagation problems to highlight the behavioral difference of functionally graded material beams with pure metal or pure ceramic beams. Batra *et al.* (2005) studied natural frequencies of a functionally graded anisotropic rectangular plate. Birman *et al.* (2007) studied the effect of damage on the free and forced vibrations of a functionally graded cantilever beam. Yang *et al.* (2008) studied the free vibration and buckling analyses of functionally graded beams with edge cracks. They conducted a detailed parametric study to show the influences of the location and total number of cracks, material properties, slenderness ratio and end supports on the flexural vibration and buckling characteristics of cracked FGM beams. Li *et al.* (2008) presented a unified approach for analyzing the static and dynamic behaviors of functionally graded Timoshenko and Euler-Bernoulli beams. Sina *et al.* (2009) presented an analytical method for the free vibration analysis of functionally graded beams. They derived the governing equations of motion using Hamilton's principle and investigated the effects of boundary conditions, volume fraction and shear deformation on the natural frequencies and mode shapes. Alshorbagy *et al.* (2011) studied free vibration characteristics of a functionally graded beam by finite element method where-in linear strain displacement relationship was considered. Ke *et al.* (2010) presented an analytical study on the nonlinear vibration of functionally graded beams.

Buckling aspects of isotropic homogenous beams, plates and shells are exhaustively reported by Timoshenko and Gere (1970). Thivend *et al.* (2008) carried out the thermal post-buckling analysis of the FGM beams through an analytical model to determine the deflection of a simply supported beam with axially immovable ends for temperatures ranging from pre-buckling to post-buckling temperatures. Sung *et al.* (2008) carried out the buckling analysis of the FGM plates and shells using a four noded quasi-conforming shell finite element. Thermal buckling and nonlinear flutter behavior of the FGM panels has been reported by Hesham *et al.* (2007). Deschilder *et al.* (2006) carried out non-linear static analysis of a FGM beam. Sang *et al.* (2007) carried out study on thermal stability boundary of FG panel under aerodynamic load. Prakash *et al.* (2006) investigated axisymmetric free flexural vibrations and thermal stability behaviors of functionally graded caps

using a three noded axisymmetric curved shell element based on field consistency approach. Jabbari *et al.* (2008) presented an analytical method to obtain the transient thermal and mechanical stresses in a functionally graded hollow cylinder subjected to two dimensional asymmetric loads. They solved the Navier's equations using a direct method of series expansion.

Thermal post-buckling analysis of slender homogenous isotropic columns (beams) using Galerkin finite element formulation is reported by Rao *et al.* (1977). Rao *et al.* (1984, 2002) also studied thermal post-buckling of homogenous columns using the Rayleigh-Ritz method. In these studies, the linear critical thermal load and the corresponding non-linear thermal load parameters have been reported for simply supported, clamped, and simply supported-clamped columns. Rao *et al.* (2002, 2003) also presented a simple intuitive method to study thermal post-buckling behavior of uniform columns. Anandrao *et al.* (2010) studied thermal post-buckling of slender FGM beams using classical Rayleigh-Ritz method as well as finite element method. They obtained closed form expressions to predict thermal post-buckling behavior of FGM beams with axially immovable ends. As discussed, thermal post-buckling of slender FGM beams has been reported earlier using analytical as well as numerical methods. The study related to thermal post-buckling of shear flexible FGM beams is not available in literature.

In this paper, large amplitude free vibration and thermal post-buckling analysis of ceramic-metal FGM beams with various length to height ratios (*L/h*) is studied using finite element formulation based on Timoshenko beam theory. The non-linear strain-displacement relations based on von-Karman type geometric non-linearity are used to account for moderately large deflections. The material properties are assumed to vary according to a power law distribution across the thickness. Beam with classical boundary conditions such as hinged-hinged (H-H), clamped-clamped (C-C) and hinged-clamped (H-C), with axially immovable ends is considered. The heterogeneity of property distribution leads to the coupling of bending and extensional deformation modes and is included in this study through a coupling matrix. The governing non-linear equations are obtained using the principle of virtual work. Iterative eigenvalue analysis has been carried out to solve for the non-linear frequency. The present study also clearly brings out the effect of shear flexibility on the post-buckling response of FGM beams for various boundary conditions, *L/h* and volume fraction exponents. The Newton-Raphson iterative procedure is used to solve the algebraic non-linear equations.

2. Functionally graded material beam

In this study, a FGM beam with ceramic on top face and metal on bottom face is considered. The variation of material properties Young's modulus '*E*', shear modulus '*G*', density '*ρ*' and coefficient of thermal expansion '*α*' across the thickness of the beam is governed by a power law distribution (Hesham 2007, Prakash and Ganapathi 2006), as given in Eq. (1), with the thickness co-ordinate *z* varying between –*h*/2 to *h*/2. The volume fraction exponent *n* can take any value between 0 to ∞, with *n* = 0 and *n* = ∞ corresponding to the two extremes of completely homogenous ceramic and metal beams respectively.

$$E(z) = E_c V_c + E_m (1 - V_c)$$
$$G(z) = G_c V_c + G_m (1 - V_c)$$
$$\rho(z) = \rho_c V_c + \rho_m (1 - V_c)$$

Table 1 Material properties of ceramic and metal

Property	Ceramic	Metal
Young's modulus E (MPa)	151000	70000
Poisson's ratio ν	0.3	0.3
ρ (kg/m^3)	5000	2780
α (10^{-06} °/° m)	10	23

$$\alpha(z) = \alpha_c V_c + \alpha_m (1 - V_c)$$

$$V_c = \left(0.5 + \frac{z}{h}\right)^n \tag{1}$$

where subscripts '*c*' and '*m*' represent ceramic and metal respectively and parameter '*V*' represent volume fraction. A FGM beam with unit height and varying lengths and with the material properties as given in Table 1 is considered for this study.

3. Finite element formulation

A finite element formulation based on first order Timoshenko beam theory is developed in this section. The non-linear equations with the consideration of large deflections are derived for FGM beam.

3.1 Displacement field - nodal displacement relation

In the present formulation, Lagrange linear interpolation functions (ψ_i) are used for interpolation of axial displacement (u), lateral displacement (w) and rotation (ϕ). The degrees of freedom vector can be expressed as

$$\left.\begin{aligned} u(x) &= \psi_1 u_1 + \psi_2 u_2 \\ w(x) &= \psi_1 w_1 + \psi_2 w_2 \\ \phi(x) &= \psi_1 \phi_1 + \psi_2 \phi_2 \end{aligned}\right\} \tag{2}$$

where '*x*' is the coordinate along length of beam.

3.2 Non-linear strain - displacement relation

By considering von-Karman type geometric non-linearity, where moderately large deflections, which are of the order of beam thickness and by neglecting non-linear axial strain term $(du_0/dx)^2$ (when the ends are immovable axially), the strain-displacement relations for the shear flexible beam can be written as

$$\varepsilon_{xx} = \frac{du_0}{dx} + \frac{1}{2}\left(\frac{dw_0}{dx}\right)^2 - z\frac{d\phi_x}{dx} \tag{3}$$

and the transverse shear strain is given by

$$\gamma_{xz} = \phi_x + \frac{dw_0}{dx} \tag{4}$$

3.3 Stress - strain relations

The axial stress σ_{xx} and axial strain ε_{xx} are related by equation

$$\sigma_{xx} = E(z)\varepsilon_{xx} \tag{5}$$

The transverse shear stress τ_{xz} and shear strain γ_{xz} are related by equation

$$\tau_{xz} = G(z)\gamma_{xz} \tag{6}$$

3.4 Stress resultant and moment resultant - displacement relations

The stress resultant N_{xx} and moment resultant M_{xx} in the axial direction can be expressed as

$$\left.\begin{aligned}
N_{xx} &= \left[\frac{du_0}{dx} + \frac{1}{2}\left(\frac{dw_0}{dx}\right)^2\right]A_{11} + \frac{d\phi_x}{dx}B_{11} - N_{xx}^T \\
M_{xx} &= \left[\frac{du_0}{dx} + \frac{1}{2}\left(\frac{dw_0}{dx}\right)^2\right]B_{11} + \frac{d\phi_x}{dx}D_{11} - M_{xx}^T
\end{aligned}\right\} \tag{7}$$

where N^T and M^T are thermal stress and moment resultants. The stiffnesses A_{11}, B_{11} and D_{11} are extensional, extension-bending coupling and bending stiffness as given by

$$\left.\begin{aligned}
A_{11} &= \int_{-h/2}^{h/2} E(z)dz \\
B_{11} &= \int_{-h/2}^{h/2} E(z)z\,dz \\
D_{11} &= \int_{-h/2}^{h/2} E(z)z^2\,dz
\end{aligned}\right\} \tag{8}$$

and shear stress resultant is

$$Q_x = K_s A_{55}\left(\frac{dw_0}{dx} + \phi_x\right) \tag{9}$$

where K_s (= 5/6) is shear correction factor. The shear stiffness is

$$A_{55} = \int_{-h/2}^{h/2} G(z)dz \tag{10}$$

where G is shear modulus. For the post-buckling analysis, the equivalent mechanical load P

developed in the beam due to temperature rise t from initial stress free temperature, for unit width of beam is given by

$$P = \int_{-h/2}^{h/2} E(z)\alpha(z)t\,dz \tag{11}$$

3.5 Governing differential equations

The governing differential equations of the first order shear deformation theory are given by

$$
\left.
\begin{aligned}
-\frac{\partial N_{xx}}{\partial x} + I_0\frac{\partial^2 u_0}{\partial t^2} + I_1\frac{\partial^2 \phi_x}{\partial t^2} + f(x) &= 0 \\[2mm]
-\frac{\partial Q_x}{\partial x} - \frac{\partial}{\partial x}\left(N_{xx}\frac{\partial w_0}{\partial x}\right) + I_0\frac{\partial^2 w_0}{\partial t^2} - q(x) &= 0 \\[2mm]
-\frac{\partial M_{xx}}{\partial x} + I_2\frac{\partial^2 \phi_x}{\partial t^2} + I_1\frac{\partial^2 u_0}{\partial t^2} + Q_x &= 0
\end{aligned}
\right\} \tag{12}
$$

where $f(x)$ is generalized axial load, $q(x)$ is generalized transverse load, Q is transverse shear and I_i are the mass moments of inertia defined by

$$
\begin{Bmatrix} I_0 \\ I_1 \\ I_2 \end{Bmatrix} = \int_{-h/2}^{h/2} \begin{Bmatrix} 1 \\ z \\ z^2 \end{Bmatrix} \rho_0 dz \tag{13}
$$

3.6 Virtual weak statements

The finite element system of equations to study the non-linear vibrations and thermal post-buckling of shear flexible FGM beam are derived by using principle of virtual work. The weak forms of governing differential equations can be obtained from Reddy (2003, 2004) as given in Eq. (14) below.

$$
\int_{\Omega^e} \frac{\partial(\delta u_0)}{\partial x} \left\{ \left[\frac{\partial u_0}{\partial x} + \frac{1}{2}\left(\frac{\partial w_0}{\partial x}\right)^2 \right] A_{11} + \frac{\partial \phi_x}{\partial x} B_{11} \right\} dx - \int_{\Omega^e} \frac{\partial(\delta u_0)}{\partial x} N_{xx}^T dx - \oint_{\Gamma^e} N_n \delta u_0 ds +
$$

$$
\int_{\Omega^e} \left(I_0 \frac{\partial^2 u_0}{\partial t^2} + I_1 \frac{\partial^2 \phi_x}{\partial t^2} \right) \delta u_0 dx = 0
$$

$$
K_s \int_{\Omega^e} \frac{\partial(\delta w_0)}{\partial x} A_{55}\left(\frac{\partial w_0}{\partial x} + \phi_x\right) dx + \int_{\Omega^e} \frac{\partial(\delta w_0)}{\partial x} \left\{ \frac{\partial w_0}{\partial x} A_{11}\left[\frac{\partial u_0}{\partial x} + \frac{1}{2}\left(\frac{\partial w_0}{\partial x}\right)^2 \right] + B_{11}\frac{\partial \phi_x}{\partial x} \right\} dx
$$

$$
-\frac{\partial(\delta w_0)}{\partial x} N_{xx}^T \frac{\partial w_0}{\partial x} dx - \delta w_0 q dx - \oint_{\Gamma^e} V_n \delta w_0 ds + \int_{\Omega^e} I_0 \frac{\partial^2 w_0}{\partial t^2} \delta w_0 dx = 0
$$

$$\int_{\Omega^e} \frac{\partial(\delta\phi_x)}{\partial x} \left\{ B_{11}\left[\frac{\partial u_0}{\partial x} + \frac{1}{2}\left(\frac{\partial w_0}{\partial x}\right)^2\right] + D_{11}\frac{\partial\phi_x}{\partial x} + K_s\delta\phi_x A_{55}\left(\frac{\partial w_0}{\partial x}+\phi_x\right)\right\} dx$$

$$-\int_{\Omega^e} \frac{\partial(\delta\phi_x)}{\partial x} M_{xx}^T dx - \oint_{\Gamma^e} M_n\delta\phi_n ds + \int_{\Omega^e}\left(I_2\frac{\partial^2\phi_x}{\partial t^2} + I_1\frac{\partial^2 u_0}{\partial t^2}\right)\delta\phi_x dx = 0 \qquad (14)$$

where δu_0, δw_0 are virtual displacements and $\delta\phi$ is virtual rotation. The secondary variables of the formulation are

$$N_n = N_{xx}n_x$$

$$V_n = Q_n + \frac{dM_{ns}}{ds}$$

$$M_n = M_{xx}n_x$$

$$P = N_{xx}\frac{dw_0}{dx}n_x \qquad (15)$$

and n_x denotes the direction cosine of the unit normal on the element boundary Γ^e.

The virtual work statements above contains at the most only the first derivatives of the dependent variables (u, w, ϕ). They can all be approximated using Lagrange interpolation functions as given in Eq. (2). Substituting expressions for u, w and ϕ from Eq. (2) in the weak form and rearranging, the finite element system of equations to study non-linear vibration and post-buckling can be expressed as

$$\begin{bmatrix} [K^{11}] & [K^{13}] & [K^{14}] \\ [K^{31}] & [K^{33}] & [K^{34}] \\ [K^{41}] & [K^{43}] & [K^{44}] \end{bmatrix}\begin{Bmatrix} \{u^e\} \\ \{w^e\} \\ \{\phi^e\} \end{Bmatrix} + \begin{bmatrix} [M^{11}] & [0] & [M^{14}] \\ [0] & [M^{33}] & [0] \\ [M^{14}]^T & [0] & [M^{44}] \end{bmatrix}\begin{Bmatrix} \{\ddot{u}^e\} \\ \{\ddot{w}^e\} \\ \{\ddot{\phi}^e\} \end{Bmatrix} = \begin{Bmatrix} F^1 \\ F^3 \\ F^4 \end{Bmatrix} + \begin{Bmatrix} F^{1T} \\ F^{3T} \\ F^{4T} \end{Bmatrix} \qquad (16)$$

The above equation can be expressed in compact matrix form as

$$[K^e]\{\Delta^e\} + [M^e]\{\ddot{\Delta}^e\} = [F^e] \qquad (17)$$

where $[K^e]$ is non-linear stiffness matrix, $[M^e]$ is the mass matrix and $[F^e]$ is force vector as given in Appendix. For Timoshenko beam elements, when linear interpolation of the lateral deflection and rotation is used, the elements do not accurately represent the bending behavior as L/h ratio becomes large. For slender beams, the transverse shear strain is required to vanish and the beam elements with linear interpolation become excessively stiff, giving rise to shear locking. In the present study, the phenomenon of shear locking is alleviated by evaluating stiffness coefficients associated with transverse shear deformation (A_{55}) using reduced integration and full integration is used for all other stiffness coefficients. For example, in $[K^{44}]$, the stiffness term containing A_{55} requires 2-point numerical integration to evaluate the integral exactly. However, this term is evaluated by using 1-point numerical integration to avoid shear locking. For free vibration study, the force vector $[F^e]$ is zero and for thermal post-buckling study, the inertia term in Eq. (17) is zero.

4. Non-linear vibration of FGM beams

FGM beam with four different L/h ratios is considered to see the effect of shear flexibility on non-linear vibrations. A convergence study was carried out with different number of elements to obtain the non-linear frequency for volume fraction exponent of unity ($n = 1.0$). The results with 50 elements along the length are found to be converged and are used for the further study. The maximum amplitude of vibration a is normalized with respect to the radius of gyration r. The values of frequency ratio are corrected to compensate for the error involved in Simple Harmonic Motion (SHM) assumption by applying Harmonic Balance Method (HBM) well reported in literature (Gupta 2009).

4.1 Solution technique

The homogenous beam vibrates with equal amplitudes at positive and negative cycles. For FGM beams, bending-extension coupling exists due to the heterogeneous material distribution through the thickness. This will result in different amplitudes of vibration at positive and negative cycles for FGM beams. Since the energy required in each deflection cycle is same, the non-linear frequency of FGM beams is obtained by computing the period of both positive and negative deflection cycles. The following iterative procedure (Mei 1973, Kitipornchai 2009) with an equivalent linearization technique is used for solving the non-linear vibration problem.

1) The basic idea is to replace the displacement dependent non-linear geometric stiffness matrix $[K^e]$ in Eq. (17) by an equivalent matrix using the mode shape of the linear vibration problem as the first approximation to the displacement.
2) This reduces the non-linear system of equations of motion to a linearized equation that can be solved as a standard eigenvalue problem.
3) The modeshape obtained by solving this eigenvalue problem can be scaled up to obtain the maximum transverse displacement equal to a given vibration amplitude a. This modeshape may be used to recompute non-linear geometric stiffness matrix $[K^e]$ for the next iteration.
4) The iterative procedure can be continued until the non-linear frequency converges to the desired accuracy (10^{-4}). This gives the non-linear half cycle frequency $\omega(+)$ for the positive deflection cycle. With this mode shape on the positive deflection cycle, maximum energy can be computed.
5) To calculate the non-linear half cycle frequency $\omega(-)$ for the negative deflection cycle, steps 1-4 are repeated with different values of negative amplitude till the energy during the negative deflection cycle is the same as that obtained during the positive deflection cycle.
6) The periods $T(+)$ and $T(-)$ at positive and negative deflection cycles are given as

$$T(+) = \frac{\pi}{\omega(+)} \quad \text{and} \quad T(-) = \frac{\pi}{\omega(-)}$$

7) The non-linear frequency for the chosen volume fraction exponent n and maximum amplitude of vibration a is

$$\omega_{NL} = \frac{2\pi}{T(+) + T(-)}$$

Table 2 Comparison of fundamental frequency (rad) for various boundary conditions

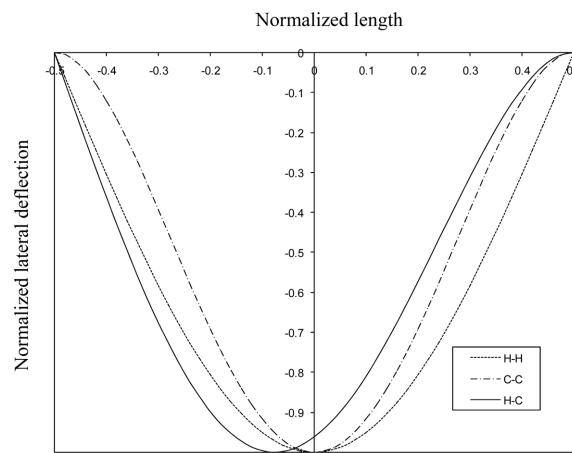|	H-H		C-C		H-C	
L/h	Present	ANSYS	Present	ANSYS	Present	ANSYS
5	588.7620	588.7325	1142.9000	1142.4285	853.2197	852.9714
10	154.0739	154.0620	333.0720	332.8411	235.5451	235.4565
50	6.2617	6.2611	14.1753	14.1636	9.7763	9.7717
100	1.5662	1.5660	3.5512	3.5482	2.4470	2.4459

Fig. 1 Mode shapes for various boundary conditions

4.2 Validation of formulation

The formulation developed for this study is validated by comparing the fundamental frequency with the fundamental frequency obtained from commercial finite element software ANSYS® for linear analysis. A homogenous ceramic beam with unit depth is modeled. The comparison of linear frequency is tabulated for various boundary conditions as given in Table 2.

An excellent match is observed between these results. Fig. 1 shows normalized lateral deformations (mode shape) along the length of the beam obtained from the present formulation for hinged-hinged, clamped-clamped and hinged-clamped beams for homogenous case ($n = 0$).

4.3 Results of vibration analysis

After validating the formulation for the homogenous beams, the non-linear vibrations of the FGM beam is studied. Fig. 2 to Fig. 13 show the plots of non-linear frequency ratio for maximum lateral deformation on positive and negative half cycle for H-H, C-C and H-C beams for different volume fraction exponents and length to height ratios. For homogenous beam ($n = 0.0$), the amplitude of vibration is identical for positive and negative half cycle for a given frequency ratio for all the boundary conditions and L/h ratios considered. For FGM beam, however, the amplitude of vibration is different for positive and negative half cycle for the same frequency ratio. The non-linear frequency ratio for a given lateral deflection (positive and negative cycle) is observed to be identical
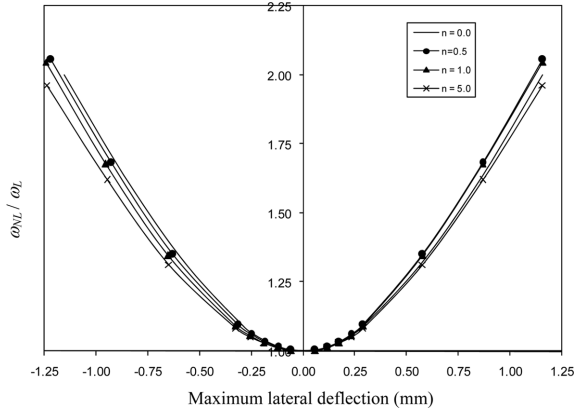
Fig. 2 Maximum lateral deflection vs. non-linear frequency ratio (H-H, *L/h* = 100)
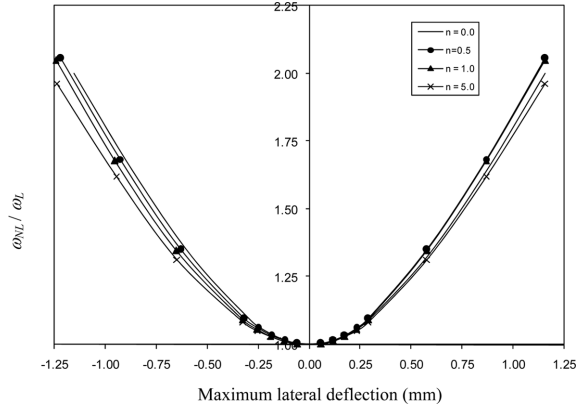
Fig. 3 Maximum lateral deflection vs. non-linear frequency ratio (H-H, *L/h* = 50)
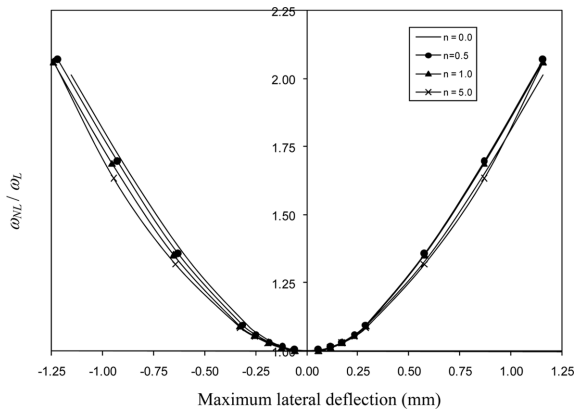
Fig. 4 Maximum lateral deflection vs. non-linear frequency ratio (H-H, *L/h* = 10)
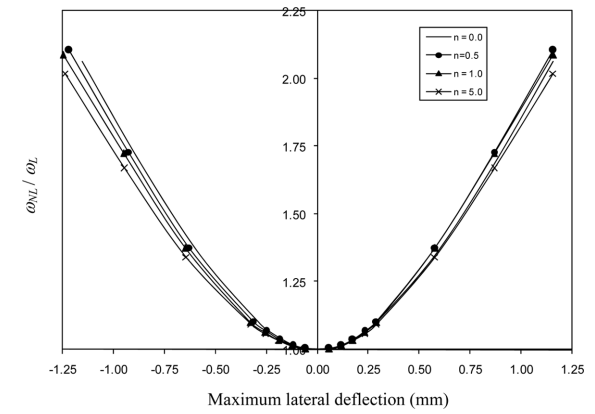
Fig. 5 Maximum lateral deflection vs. non-linear frequency ratio (H-H, *L/h* = 5)
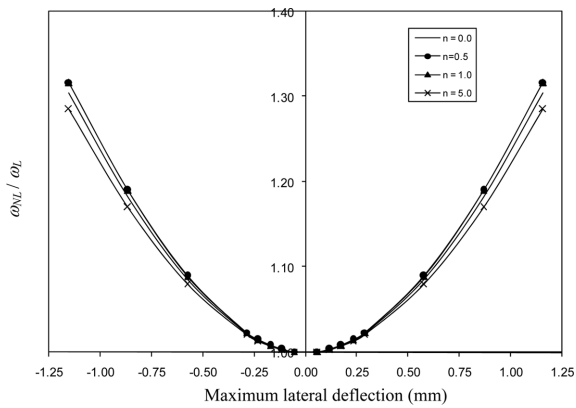

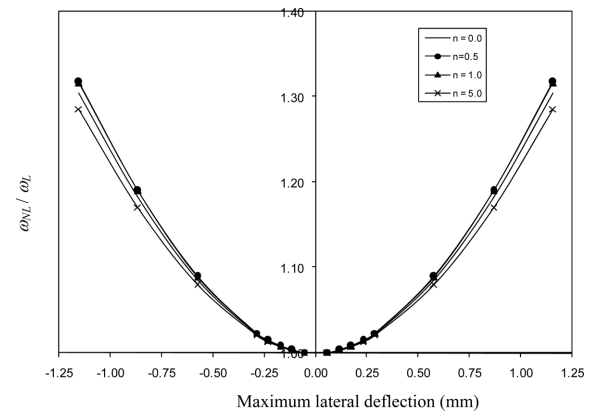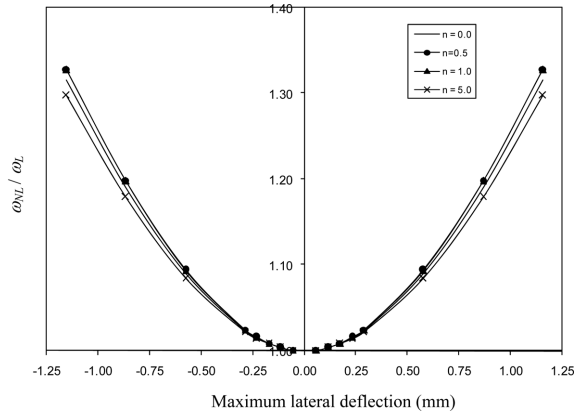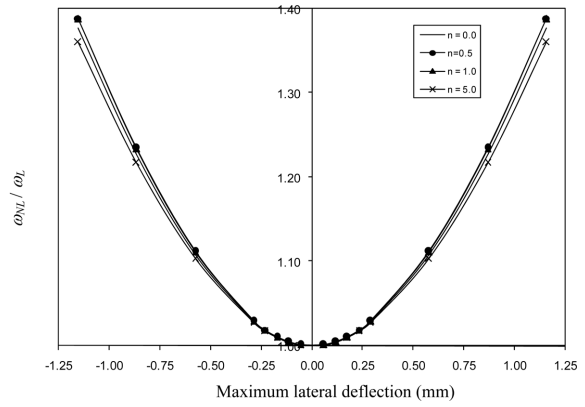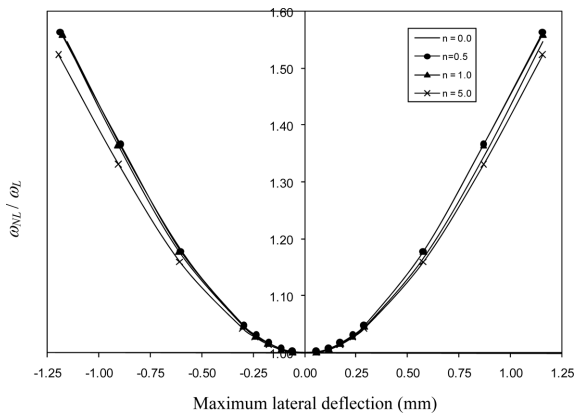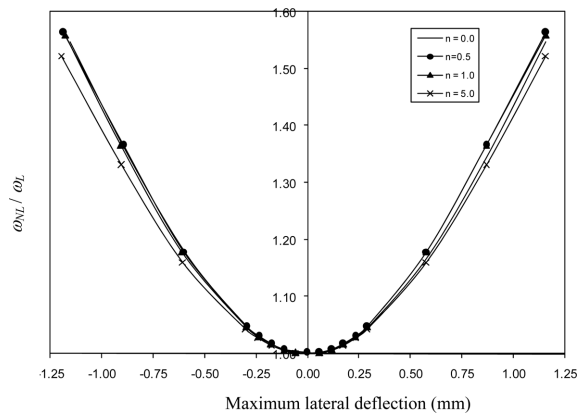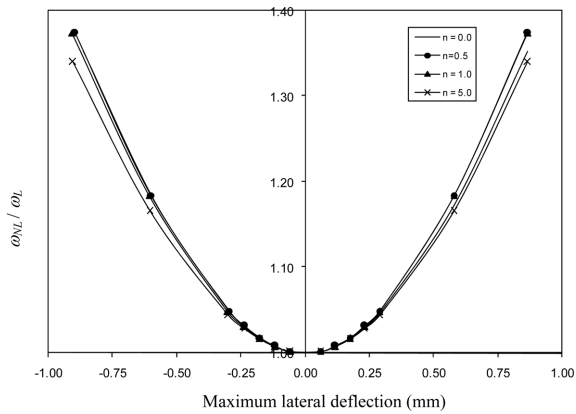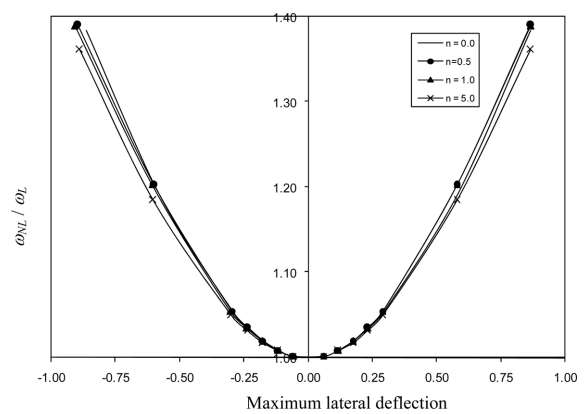Fig. 6 Maximum lateral deflection vs. non-linear frequency ratio (C-C, *L/h* = 100)

Fig. 7 Maximum lateral deflection vs. non-linear frequency ratio (C-C, *L/h* = 50)

Fig. 8 Maximum lateral deflection vs. non-linear frequency ratio (C-C, *L/h* = 10)

Fig. 9 Maximum lateral deflection vs. non-linear frequency ratio (C-C, *L/h* = 5)

Fig. 10 Maximum lateral deflection vs. non-linear frequency ratio (H-C, *L/h* = 100)

Fig. 11 Maximum lateral deflection vs. non-linear frequency ratio (H-C, *L/h* = 50)

Fig. 12 Maximum lateral deflection vs. non-linear frequency ratio (H-C, *L/h* = 10)

Fig. 13 Maximum lateral deflection vs. non-linear frequency ratio (H-C, *L/h* = 5)

K. Sanjay Anandrao, R.K. Gupta, P. Ramchandran and G. Venkateswara Rao

Table 3 Frequency ratio for various *a*, Hinged-Hinged Beam (*n* = 1.0)

L/h = 100		L/h = 50	
a	ω_{NL}/ω_L	*a*	ω_{NL}/ω_L
-1.245	2.047	-1.245	2.048
-0.954	1.679	-0.954	1.679
-0.654	1.346	-0.654	1.347
-0.330	1.091	-0.330	1.091
-0.261	1.057	-0.261	1.057
-0.192	1.031	-0.192	1.031
-0.125	1.013	-0.125	1.013
-0.060	1.003	-0.060	1.003
0.058	1.003	0.058	1.003
0.115	1.013	0.115	1.013
0.173	1.031	0.173	1.031
0.231	1.057	0.231	1.057
0.289	1.091	0.289	1.091
0.577	1.346	0.577	1.347
0.866	1.679	0.866	1.679
1.154	2.047	1.154	2.048

Table 4 Frequency ratio for various *a*, Clamped-Clamped Beam (*n* = 0.5)

L/h = 100		L/h = 50	
a	ω_{NL}/ω_L	*a*	ω_{NL}/ω_L
-1.154	1.317	-1.154	1.318
-0.866	1.191	-0.866	1.191
-0.577	1.089	-0.577	1.090
-0.289	1.023	-0.289	1.023
-0.231	1.015	-0.231	1.015
-0.173	1.008	-0.173	1.008
-0.115	1.004	-0.115	1.004
-0.058	1.001	-0.058	1.001
0.058	1.001	0.058	1.001
0.115	1.004	0.115	1.004
0.173	1.008	0.173	1.008
0.231	1.015	0.231	1.015
0.289	1.023	0.289	1.023
0.577	1.089	0.577	1.090
0.866	1.191	0.866	1.191
1.154	1.317	1.154	1.318

Table 5 Frequency ratio for various *a*, Hinged-Clamped Beam (*n* = 5)

$L/h = 100$		$L/h = 50$	
a	ω_{NL}/ω_L	*a*	ω_{NL}/ω_L
-1.198	1.523	-1.198	1.523
-0.905	1.331	-0.905	1.331
-0.607	1.160	-0.607	1.161
-0.301	1.042	-0.301	1.042
-0.239	1.027	-0.239	1.027
-0.178	1.015	-0.178	1.015
-0.118	1.007	-0.118	1.007
-0.058	1.002	-0.058	1.002
0.058	1.002	0.058	1.002
0.115	1.007	0.115	1.007
0.173	1.015	0.173	1.015
0.231	1.027	0.231	1.027
0.289	1.042	0.289	1.042
0.577	1.160	0.577	1.161
0.866	1.331	0.866	1.331
1.154	1.523	1.154	1.523

Table 6 Frequency ratio for various *a*, *n* = 0.5 and *L/h* = 50

H-H		C-C		H-C	
a	ω_{NL}/ω_L	*a*	ω_{NL}/ω_L	*A*	ω_{NL}/ω_L
-1.2193	2.0563	-1.1544	1.3175	-1.1860	1.5638
-0.9281	1.6835	-0.8658	1.1907	-0.8962	1.3664
-0.6317	1.3501	-0.5772	1.0895	-0.6010	1.1791
-0.3178	1.0953	-0.2886	1.0232	-0.2989	1.0475
-0.2525	1.0607	-0.2309	1.0149	-0.2378	1.0305
-0.1866	1.0336	-0.1732	1.0084	-0.1773	1.0172
-0.1219	1.0146	-0.1154	1.0038	-0.1174	1.0076
-0.0593	1.0035	-0.0577	1.0009	-0.0058	1.0019
0.0577	1.0035	0.0577	1.0009	0.0577	1.0019
0.1154	1.0146	0.1154	1.0038	0.1154	1.0076
0.1732	1.0336	0.1732	1.0084	0.1732	1.0172
0.2309	1.0607	0.2309	1.0149	0.2309	1.0305
0.2886	1.0953	0.2886	1.0232	0.2886	1.0475
0.5772	1.3501	0.5772	1.0895	0.5772	1.1791
0.8658	1.6835	0.8658	1.1907	0.8658	1.3664
1.1544	2.0563	1.1544	1.3175	1.1544	1.5638

for higher L/h ratio for the boundary condition considered. Typical values of maximum amplitude and non-linear frequency ratio for various boundary conditions are shown in Table 3, Table 4 and Table 5.

For clamped-clamped FGM beam, there is no effect of bending-extension coupling on vibration. For this boundary condition, the non-linear frequency ratio is identical for positive and negative amplitude of vibration cycle as shown in Table 4. This is also evident from Fig. 6 to Fig. 9 wherein the graphs are symmetric about Y-axis.

For given amplitude of vibration, the effect of non-linearity is observed more for hinged-hinged beam as compared to clamped-clamped and hinged-clamped beams. For hinged-clamped beam, the effect of non-linearity is in between that for hinged-hinged and clamped-clamped beams. A typical comparison of amplitude of vibration and frequency ratio is shown in Table 6 for volume fraction index $n = 0.5$ and $L/h = 50$.

5. Thermal post-buckling of FGM beams

The thermal load is applied as temperature rise from initial stress free temperature. The properties are assumed to be independent of temperature.

5.1 Solution technique (Newton-Raphson solution)

The assembled non-linear finite element system of equations (Eq. (17)) can be written as

$$K(\Delta)\Delta = F \tag{18}$$

where Δ represents the matrix of unknown degrees of freedom. The residual is

$$R = K(\Delta)\Delta - F \tag{19}$$

The load step is given in terms of the temperature increment t from the previous converged solution. Using the Newton-Raphson algorithm, for the rth iteration

$$\Delta^{r+1} = \Delta^r - (T^r)^{-1} R^r \tag{20}$$

where the tangent stiffness matrix is given by

$$T^r = \frac{\partial R^r}{\partial \Delta} \tag{21}$$

The iterative procedure is terminated when the Euclidean norm of the residual vector (L_2) is lower than the specified tolerance ε.

$$\sqrt{\sum_{i=1}^{n} R_i^2} \le \varepsilon \tag{22}$$

5.2 Results of thermal post-buckling

5.2.1 Hinged-hinged beam (H-H)

The results obtained from present formulation (Timoshenko beam) are plotted along with the results obtained from Anandrao (2010, Euler-Bernoulli beam). Fig. 14 and Fig. 15 shows the post-buckling load deflection path for length to height ratios $L/h = 100$ and $L/h = 50$ respectively. The normalized thermal load $\lambda \ (= t \ (L/h)^2 \ \alpha_m)$ in terms of temperature (t) increment from initial stress free temperature is plotted along x-axis. The normalized maximum lateral deflection occurring at mid-length (W_{max}/L) is plotted along y-axis. As can be observed from the figures, the load-deflection paths obtained from both formulations (Timoshenko and Euler-Bernoulli) show a close match for all the volume fraction exponents considered. However, for $L/h = 10$, as shown in Fig. 16, the two
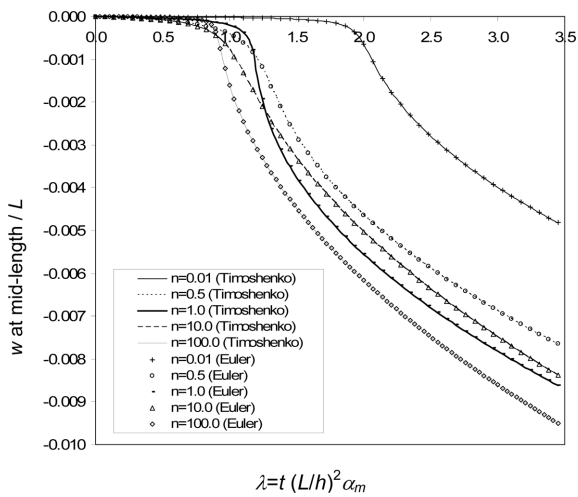

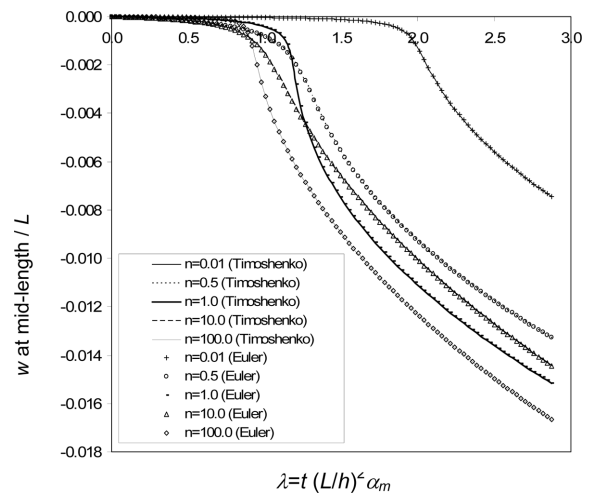Fig. 14 Post-buckling load vs. deflection curves for FGM beams (H-H, $L/h = 100$)

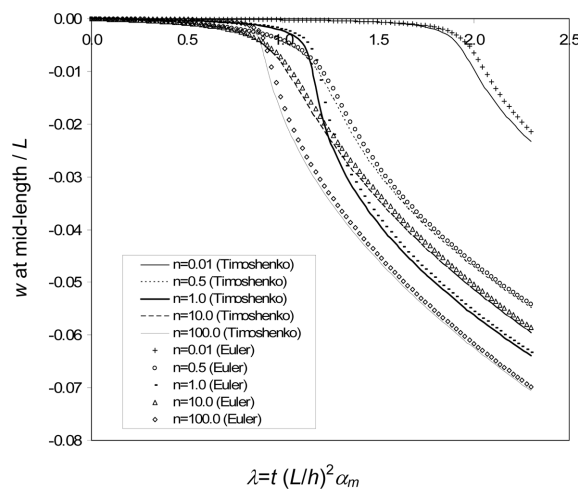Fig. 15 Post-buckling load vs. deflection curves for FGM beams (H-H, $L/h = 50$)

Fig. 16 Post-buckling load vs. deflection curves for FGM beams (H-H, $L/h = 10$)

load-deflection paths do not match showing the effect of shear flexibility. When the effect of shear flexibility is considered, the beam starts deforming from its equilibrium position at lower temperature than the case when shear flexibility effects are neglected. Further, it can be observed that for all the ratios of L/h considered in the study, the beam started deviating from the equilibrium position even for a small temperature increment from the initial stress free temperature. This phenomenon is in agreement with the observations made by Anandrao (2010) for slender beams where no sudden transverse deflection (buckling) is observed for H-H FGM beam.

An eigenvalue buckling analysis was carried out using general purpose finite element software ANSYS® for completely ceramic beam and completely metallic beam for different L/h. The purpose of this analysis was to obtain the critical temperatures for the above materials for the various L/h considered. The results are summarized in Table 7.

By using the formulations developed, completely ceramic beam was modeled by considering volume fraction exponent $n = 0.01$ and completely metallic beam was modeled by considering $n = 100.0$. The load-deflection curves for these two cases clearly show sudden increase in deflection

Table 7 Normalized critical thermal load for homogenous beams (H-H)

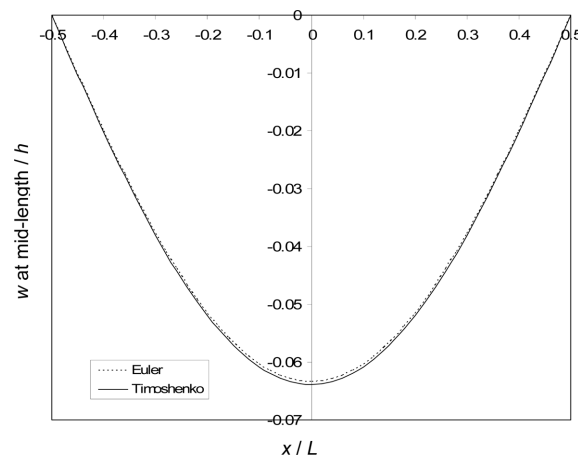| L/h	Ceramic	Ceramic	Metal	Metal
	Euler	Timoshenko	Euler	Timoshenko
10	1.8911	1.8447	0.8222	0.8021
50	1.8917	1.8898	0.8225	0.8216
100	1.8917	1.8913	0.8225	0.8223

Fig. 17 Buckled mode shape for FGM beam, $n = 1.0$, $L/h = 10$, $\lambda = 2.3$, H-H

Table 8 % error in maximum lateral deflection for neglecting shear effects (H-H)

L/h	$n = 0.1$	$n = 0.5$	$n = 1.0$	$n = 10.0$	$n = 100.0$
10	8.23	1.17	0.81	1.70	1.01
50	0.11	0.08	0.07	0.07	0.06
100	0.01	0.05	0.05	0.03	0.03

near the critical temperatures tabulated in Table 7. Fig. 17 shows buckled mode shape for $L/h = 10$ and $n = 1.0$ at $\lambda = 2.3$. Table 8 shows the % error in maximum lateral deflection at $\lambda = 2.3$ for neglecting shear effects. As can be observed from the table, as the L/h ratio is increased beyond 50, the effect of shear flexibility on lateral deflection can be neglected.

5.2.2 Clamped-clamped beam (C-C)

Similar study was carried out for FGM beam with clamped ends. Fig. 18 and Fig. 19 shows the post-buckling load deflection path for length to height ratios $L/h = 100$ and $L/h = 50$ respectively. As can be observed from the figures, the load-deflection paths obtained from both formulations (Euler-Bernoulli and Timoshenko) show a fairly close match for all the volume fraction exponents
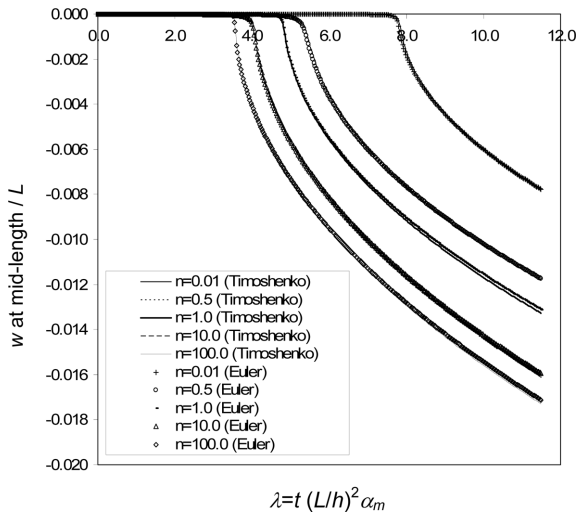

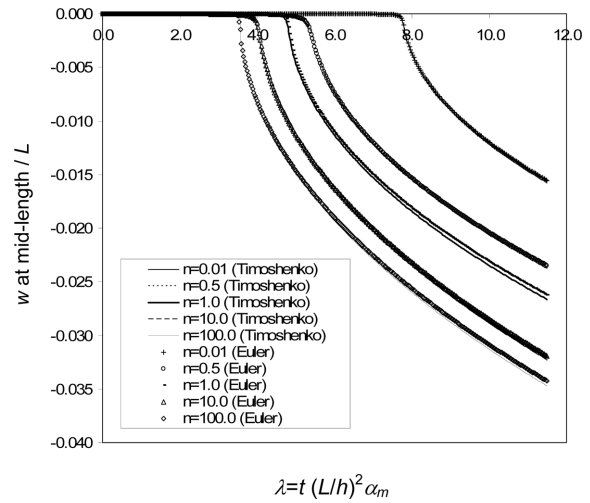Fig. 18 Post-buckling load vs. deflection curves for FGM beams (C-C, $L/h = 100$)

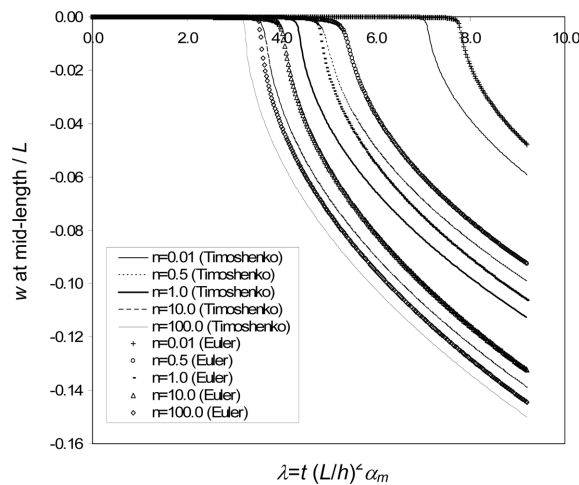Fig. 19 Post-buckling load vs. deflection curves for FGM beams (C-C, $L/h = 50$)

Fig. 20 Post-buckling load vs. deflection curves for FGM beams (C-C, $L/h = 10$)

Table 9 Normalized critical thermal load for homogenous beams (C-C)

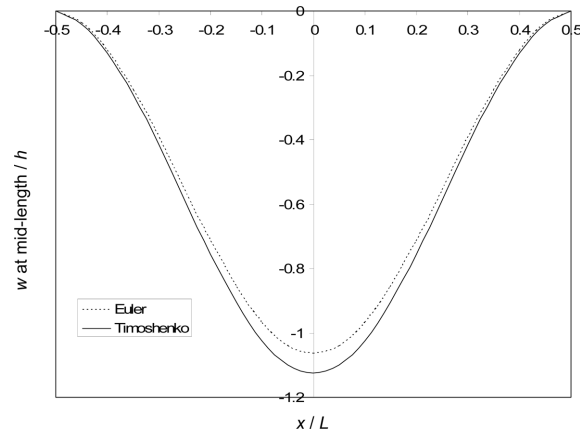| L/h	Ceramic Euler	Ceramic Timoshenko	Metal Euler	Metal Timoshenko
10	7.5670	6.8494	3.2890	2.9785
50	7.5667	7.5337	3.2899	3.2764
100	7.5668	7.5590	3.2899	3.2865

Fig. 21 Buckled mode shape for FGM beam, n = 1.0, L/h = 10, λ = 9.2, C-C

Table 10 % error in maximum lateral deflection for neglecting shear effects (C-C)

L/h	n = 0.1 Euler	n = 0.5 Euler	n = 1.0 Euler	n = 10.0 Euler	n = 100.0 Euler
10	18.98	6.57	5.38	4.71	3.66
50	1.34	1.29	1.37	1.34	1.34
100	0.57	0.89	1.03	1.13	1.01

considered. However, for L/h = 10, as shown in Fig. 20, the two load-deflection paths do not match showing the effect of shear flexibility. Similar to hinged beam, when the effect of shear flexibility is considered, the beam starts deforming from its equilibrium position at lower temperature than the case when shear flexibility effects are neglected. The FGM beam with clamped ends shows critical bifurcation temperature for both formulations, all volume fraction exponents and all L/h considered.

An eigenvalue buckling analysis was carried out using ANSYS® for completely ceramic beam and completely metallic beam with clamped ends. The results are summarized in Table 9. The load-deflection curves for n = 0.01 and n = 100.0 clearly show bifurcation temperatures at the above temperatures. Fig. 21 shows buckled mode shape for L/h = 10 and n = 1.0 at λ = 9.2. Table 10 shows the % error in maximum lateral deflection at λ = 9.2 for neglecting shear effects. As can be observed from the table, as the L/h ratio is increased beyond 50, the effect of shear flexibility on lateral deflection becomes less significant. Further, the effect of shear flexibility is observed to be more predominant for clamped beam as compared to simply supported beam.

6. Conclusions

A comprehensive study on non-linear vibration and thermal post-buckling of shear flexible FGM beams is reported in this paper. The von-Karman type of geometric non-linearity is considered. A beam with various classical boundary conditions and axially immovable ends is considered. A power law distribution is assumed for the variation of properties through the thickness. The governing non-linear equations of motion are obtained using the principle of virtual work. The effect of L/h ratio and volume fraction exponent n is clearly demonstrated.

For the non-linear vibrations of shear flexible FGM beams, an iterative procedure which consists of an equivalent linearization technique is used. The Harmonic Balance Method is used to correct for the SHM assumption involved in the formulation. The following conclusions can be drawn from the numerical results obtained from the present study.

1) Hardening type of non-linearity is observed for all the boundary conditions considered.
2) The non-linear frequency ratio for a given lateral deflection is observed to be identical for higher L/h ratio for all the boundary conditions considered.
3) Shear flexibility effects should be considered to study the non-linear vibration response of FGM beams when L/h value is small to obtain realistic response.
4) For homogenous beams, the amplitude of vibration is identical for positive and negative half cycle for a given frequency ratio.
5) For FGM beams, the non-linear frequencies are dependent on the sign of the vibration amplitudes.
6) As the effect of bending-extension coupling on vibration of clamped-clamped FGM beam is zero, the non-linear frequency ratio is identical for positive and negative amplitude of vibration cycle for this boundary condition.
7) For given amplitude of vibration, the effect of non-linearity is observed to be more for hinged-hinged beam as compared to clamped-clamped and hinged-clamped beams. For hinged-clamped beam, the effect of non-linearity is in between that for hinged-hinged and clamped-clamped beams.

For study on thermal post-buckling, load-deflection curves and buckled mode shapes are presented for various boundary conditions. It is shown based on this study that shear flexibility effects should be considered to study the post-buckling response of FGM beams, when L/h ratio is small, to obtain realistic response. Further, the effect of shear flexibility was observed to be more considerable for clamped beam as compared to simply supported beam for similar values of L/h and volume fraction exponent. It was further observed that clamped FGM beams show critical bifurcation temperature whereas simply supported FGM beams deform laterally even for small temperature increase from initial stress free temperature.

Acknowledgements

References

Aboudi, J., Pindera, M.J. and Arnold, S.M. (1999), "Higher order theory for functionally graded materials", *Compos. Part B-Eng.*, **30**, 777-832.

Alshorbagy, A.E., Eltaher, M.A. and Mahmoud, F.F. (2011), "Free vibration characteristics of a functionally graded beam by finite element method", *Applied Mathematical Modeling*, **35**, 412-425.

Anandrao, S.K., Gupta, R.K., Ramchandran, P. and Rao, G.V. (2010), "Thermal post-buckling analysis of uniform slender functionally graded material beams", *Struct. Eng. Mech.*, **36**(5), 545-560.

ANSYS Inc. ANSYS package version 10.0, Canons Burgh, PA, USA.

Batra, R.C. and Jin, J. (2005), "Natural frequencies of a functionally graded anisotropic rectangular plate", *J. Sound Vib.*, **282**, 509-516.

Birman, V. and Byrd, L.W. (2007), "Vibrations of damaged cantilever beams manufactured from functionally graded materials", *AIAA J.*, **45**(11), 2747-2757.

Chakraborty, A., Gopalkrishnan, S. and Reddy, J.N. (2003), "A new beam finite element for the analysis of functionally graded materials", *Int. J. Mech. Sci.*, **45**, 519-539.

Deschilder, M., Eslami, H. and Zhao, Y. (2006), "Non-linear static analysis of a beam made of functionally graded material", *Proceedings of 47th AIAA/ASME/ASCE/AHS/ASC Structures, Structural Dynamics, and Materials Conference*, Newport, Rhode Island.

Gupta, R.K., Jagadish, G.B., Janardhan, G.R. and Rao, G.V. (2009), "Relatively simple finite element formulation for the large amplitude free vibrations of uniform beams", *Finite Elem. Anal. Des.*, **45**, 624-631.

Hesham, H.I. (2007), "Thermal buckling and nonlinear flutter behavior of functionally graded material panels", *J. Aircraft*, **44**(5), 1610-1618.

Jabbari, M., Vaghari, A.R., Bahtui, A. and Eslami, M.R. (2008), "Exact solution for asymmetric transient thermal and mechanical stresses in FGM hollow cylinders with heat source", *Struct. Eng. Mech.*, **29**(5), 551-565.

Ke, L.L., Yang, J. and Kitipornchai, S. (2010), "An analytical study on the nonlinear vibration of functionally graded beams", *Meccanica*, **45**, 743-752.

Kitipornchai, S., Ke, L.L., Yang, J. and Xiang, Y. (2009), "Non-linear vibration of edge cracked functionally graded Timoshenko beams", *J. Sound Vib.*, **324**, 962-982.

Koizumi, M. (1993), "The concept of FGM", *Ceram. Trans.*, **34**(1), 3-10.

Li, X.F. (2008), "A unified approach for analyzing static and dynamic behaviors of functionally graded Timoshenko and Euler-Bernoulli beams", *J. Sound Vib.*, **318**, 1210-1229.

Mei, C. (1973), "Finite element analysis of non-linear vibrations of beam columns", *AIAA J.*, **11**, 115-117.

Prakash, T. and Ganapathi, M. (2006), "Asymmetric flexural vibration and thermoelastic stability of FGM plates using finite element method", *Composites: Part B*, **37**, 642-649.

Prakash, T., Singh, M.K. and Ganapathi, M. (2006), "Vibrations and thermal stability of functionally graded spherical caps", *Struct. Eng. Mech.*, **24**(4), 447-462.

Raju, K.K. and Rao, G.V. (1984), "A note on large amplitude vibrations", *Comput. Struct.*, **18**(6), 1189-1191.

Raju, K.K. and Rao, G.V. (2005), "Towards improved evaluation of large amplitude free vibration behavior of uniform beams using multi-term admissible functions", *J. Sound Vib.*, **282**, 1238-1246.

Rao, G.V. and Raju, P.C. (1977), "Post-buckling of uniform cantilever columns - Galerkin finite element formulation", *Eng. Fract. Mech.*, **9**, 1-4.

Rao, G.V. and Raju, K.K. (1978), "Large amplitude vibrations of beams with elastically restrained ends", *J. Sound Vib.*, **57**(2), 302-304.

Rao, G.V. and Raju, K.K. (1984), "Thermal post buckling of columns", *AIAA*, **22**(6), 850-851.

Rao, G.V. and Raju, K.K. (2002), "Thermal post buckling of uniform Columns: A simple intuitive method", *AIAA J.*, **40**(10), 2138-2140.

Rao, G.V. and Raju, K.K. (2002), "A direct numerical integration method to study the large amplitude vibration of slender beams with immovable ends", *J. Inst. Eng.*, **83**, 42-44.

Rao, G.V. and Raju, K.K. (2003), "A simple method to predict the thermal post-buckling behavior of columns on Pasternak foundation", *Ind. J. Eng. Mater. Sci.*, **10**, 177-182.

Rao, G.V. (2003), "A simple energy method to predict the thermal post buckling behavior of columns", *J. Aeros. Sci. Tech.*, **55**(2), 141-143.

Rao, S.S. (2007), *Vibration of Continuous System*, John Wiley & Sons, Inc.

Reddy, J.N. (2003), *Mechanics of Laminated Composite Plates and Shells: Theory and Analysis*, CRC Press, New York.

Reddy, J.N. (2004), *An Introduction to Non-linear Finite Element Analysis*, Oxford University Press, USA.

Sang-Lae, L. and Ji-Hwan, K. (2007), "Thermal stability boundary of FG panel under aerodynamic load", *Int. J. Mech. Syst. Sci. Eng.*, **1**(2), 105-110.

Sathyamoorthy, M. (1998), *Nonlinear Analysis of Structures*, CRC Mechanical Engineering Series, CRC Press, Boca Raton, 26-38.

Sina, S.A., Navazi, H.M. and Haddadpour, H. (2009), "An analytical method for free vibration analysis of functionally graded beams", *Mater. Des.*, **30**, 741-747.

Singh, G., Sharma, A.K. and Rao, G.V. (1990), "Large amplitude free vibrations of beams - a discussion on various formulations and assumptions", *J. Sound Vib.*, **142**(1), 77-85.

Singh, G., Rao, G.V. and Iyengar, N.G.R. (1990), "Re-investigation of large amplitude free vibrations of beams using finite elements", *J. Sound Vib.*, **143**, 351-355.

Srinivasan, A.V. (1965), "Large amplitude free oscillations of beams and plates", *AIAA J.*, **3**(10), 1951-1953.

Sung-Cheon, H., Gilson, R.L. and Ki-Du, K. (2008), "Mechanical vibration and buckling analysis of FGM plates and shells using a four node quasi conforming shell element", *Int. J. Struct. Stab. D.*, **8**(2), 203-229.

Thivend, J., Habib, E. and Yi, Z. (2008), "Thermal post buckling analysis of FGM beams", *49th AIAA/ASME/ASCE/AHS/ASC Structures, Structural Dynamics and Materials Conference*, AIAA 2008-2272.

Timoshenko, S.P. and Gere, J.M. (1970), *Theory of Elastic Stability*, McGraw-Hill.

Woinowsky - Krieger, S. (1950), "The effect of an axial force on the vibrations of hinged bars", *Tran. ASME, J. Appl. Mech.*, **17**, 35-36.

Yang, J. and Chen, Y. (2008), "Free vibration and buckling analyses of functionally graded beams with edge cracks", *Compos. Struct.*, **83**, 48-60.

Appendix

Non-linear stiffness matrix $[K^e]$

$$K_{ij}^{11} = \int_{\Omega^e} A_{11} \frac{d\psi_i}{dx} \frac{d\psi_j}{dx} dx$$

$$K_{ij}^{13} = \frac{1}{2} \int_{\Omega^e} \frac{d\psi_i}{dx} A_{11} \frac{dw_0}{dx} \frac{d\psi_j}{dx} dx$$

$$K_{ij}^{14} = \int_{\Omega^e} \frac{d\psi_i}{dx} B_{11} \frac{d\psi_j}{dx} dx = K_{ji}^{41}$$

$$K_{ij}^{31} = \int_{\Omega^e} \frac{d\psi_j}{dx} A_{11} \frac{dw_0}{dx} \frac{d\psi_i}{dx} dx$$

$$K_{ij}^{33} = K_s \int_{\Omega^e} \frac{d\psi_i}{dx} A_{55} \frac{d\psi_j}{dx} dx + \frac{1}{2} \int_{\Omega^e} A_{11} \left(\frac{dw_0}{dx} \right)^2 \frac{d\psi_i}{dx} \frac{d\psi_j}{dx} dx$$

$$K_{ij}^{34} = K_s \int_{\Omega^e} A_{55} \frac{d\psi_i}{dx} \psi_j dx + \int_{\Omega^e} \frac{d\psi_i}{dx} \frac{dw_0}{dx} B_{11} \frac{d\psi_j}{dx} dx$$

$$K_{ij}^{43} = K_s \int_{\Omega^e} A_{55} \frac{d\psi_j}{dx} \psi_i dx + \frac{1}{2} \int_{\Omega^e} \frac{d\psi_j}{dx} \frac{dw_0}{dx} B_{11} \frac{d\psi_i}{dx} dx$$

$$K_{ij}^{44} = \int_{\Omega^e} \frac{d\psi_i}{dx} D_{11} \frac{d\psi_j}{dx} + K_s A_{55} \psi_i \psi_j dx$$

Mass matrix $[M^e]$

$$M_{ij}^{11} = \int_{\Omega^e} I_0 \psi_i \psi_j dx$$

$$M_{ij}^{14} = -\int_{\Omega^e} I_1 \psi_i \psi_j dx$$

$$M_{ij}^{33} = -\int_{\Omega^e} I_0 \psi_i \psi_j dx$$

$$M_{ij}^{44} = -\int_{\Omega^e} I_2 \psi_i \psi_j dx$$

Load vector $[F^e]$

$$F_i^1 = \oint_{\Gamma^e} N_{xx} \psi_i ds \qquad F_i^3 = \int_{\Omega^e} q \psi_i dx \qquad F_i^4 = \oint_{\Gamma^e} M_{xx} \psi_i ds$$

$$F_i^{1T} = \oint_{\Omega^e} N_{xx}^T \frac{d\psi_i}{dx} dx \qquad F_i^{3T} = \oint_{\Omega^e} \frac{d\psi_i}{dx} N_{xx}^T \frac{dw_0}{dx} dx \qquad F_i^{4T} = \oint_{\Omega^e} \frac{d\psi_i}{dx} M_{xx}^T dx$$

Tangent stiffness matrix $[T^e]$

$$T_{ij}^{11} = K_{ij}^{11}$$

$$T_{ij}^{13} = 2K_{ij}^{13} = T_{ji}^{31}$$

$$T_{ij}^{14} = K_{ij}^{14}$$

$$T_{ij}^{33} = \int_{\Omega^e} \frac{du_0}{dx} A_{11} \frac{d\psi_j}{dx} \frac{d\psi_i}{dx} dx + \int_{\Omega^e} A_{11} \frac{dw_0}{dx} \frac{d\psi_j}{dx} \frac{d\psi_i}{dx} \frac{dw_0}{dx} dx + \int_{\Omega^e} \frac{d\psi_i}{dx} \frac{d\psi_j}{dx} B_{11} \frac{d\varphi_x}{dx} dx + K_{ij}^{33}$$

$$T_{ij}^{34} = K_{ij}^{34}$$

$$T_{ij}^{41} = K_{ij}^{41}$$

$$T_{ij}^{43} = \frac{1}{2} \int_{\Omega^e} \frac{dw_0}{dx} \frac{d\psi_j}{dx} B_{11} \frac{d\psi_i}{dx} dx + K_{ij}^{43}$$

$$T_{ij}^{44} = K_{ij}^{44}$$